Effect of Calcium Concentration on the Structure of Casein Micelles in Thin Films

P. Müller-Buschbaum,* R. Gebhardt,[†] S. V. Roth,[‡] E. Metwalli,* and W. Doster*
*Physik-Department, Technische Universität München, Garching, Germany; [†]European Syncrotron Radiation Facility, Grenoble, France; and [‡]HASYLAB at DESY, Hamburg, Germany

ABSTRACT   The structure of thin casein films prepared with spin-coating is investigated as a function of the calcium concentration. Grazing incidence small-angle x-ray scattering and atomic force microscopy are used to probe the micelle structure. For comparison, the corresponding casein solutions are investigated with dynamic light-scattering experiments. In the thin films with added calcium three types of casein structures, aggregates, micelles, and mini-micelles, are observed in coexistence with atomic force microscopy and grazing incidence small-angle x-ray scattering. With increasing calcium concentration, the size of the aggregates strongly increases, while the size of micelles slightly decreases and the size of the mini-micelles increases. This effect is explained in the framework of the particle-stabilizing properties of the hairy layer of κ-casein surrounding the casein micelles.

INTRODUCTION

Caseins, a family of phosphoproteins, form the largest protein component in most milks. The major function of caseins in milk is to efficiently transport calcium, phosphate, and protein from the mammary gland to the neonate (1,2). It has been suggested that casein micelles allow the total calcium and phosphate concentrations in most, if not all, milks to exceed the solubility of calcium phosphate, without causing uncontrolled precipitation of calcium phosphate in the mammary gland (3,4).

Today it is generally accepted that caseins assemble into casein micelles, the aggregates in which they are found in milk. Casein micelles are polydisperse, roughly spherical aggregates with diameters ranging between 150 and 300 nm. In contrast to conventional surfactant systems, casein micelles are heterogeneous, composed of four different proteins, α(s1)- and α(s2)-caseins, β-casein, and κ-casein (5). Structure and stability of the casein micelles is still a matter of debate and different models are discussed in literature (6–10). In the sub-micelle model, the caseins first aggregate via hydrophobic interaction into subunits of 15–20 molecules each, thereby creating a well-defined substructure on a scale of 20 nm (11–13). These units are linked by small calcium phosphate clusters, while other models deny the existence of casein sub-micelles and consider calcium phosphate clusters as seeds of micelle growth (14,15). Along this line, the dual binding model (16,17) accounts for distinct hydrophilic and hydrophobic regions of the particular polypeptides. Analogous to diblock copolymers, the hydrophobic regions associate, stabilizing the core of the micelle, and at the hydrophilic regions, the colloidal calcium phosphate particles are attached.

A consensus of opinion exists that an outer hairy layer of κ-casein ensures the stability of the casein micelle through a steric stabilization mechanism (18). The nonadsorbing part of κ-casein can be regarded as a salted polyelectrolyte brush. In the extended state, the brush is ~7 nm long and provides the steric stabilization, while in the collapsed state the stabilization is absent and flocculation and gel formation become possible (19–21). Calcium is essential for the micelle formation at all (22). The casein proteins divide themselves into two groups, the calcium-sensitive and the non-calcium-sensitive, which also in mixtures prevent or inhibit the precipitation of the calcium-sensitive group by calcium. The κ-casein is insensitive to calcium and α(s1)- and α(s2)-caseins and β-casein are calcium-sensitive.

As mentioned, the main physiological task of the caseins is to solubilize calcium phosphate during pregnancy and lactation in mammary gland. The highly phosphorylated caseins, along with many other phosphoproteins found in calcifying tissues, have been shown to be effective in inhibiting the precipitation of calcium phosphate from solutions at low to moderate supersaturation (4). Approximately one mM casein in milk binds 10 mM Ca_2PO_4 in aqueous solution, whose solubility is in the range of 10^{-3} mM. The open and flexible conformation in solution of many of these highly phosphorylated phosphoproteins is believed to be an adaptive feature of peptides required to interact speedily with calcium phosphate nuclei to control ectopic calcification in biological tissues. One of the proteins building the casein micelle, β-casein, shows a number of similarities of primary structure to the proline-rich phosphoproteins of saliva.

In milk, calcium is present in various forms (23). For a total concentration of 32 mmol/L, 22 mmol/L are in the colloidal state and 10 mmol/L are diffusible. Only 2 mmol/L of this diffusible calcium are free ionic Ca^{2+} (abbreviated ''Ca'' in this article). The remainder is essentially complexed

with citrate, phosphate, caseins, or whey proteins. In the colloidal state, calcium can be complexed with phosphoester, carboxyl groups of micellar caseins or with colloidal phosphate and citrate associated with casein micelles (24). Enrichment of milk with calcium is a common practice to improve the functional, technological, and sometimes nutritional properties of milk (25).

Whereas most investigations address solutions at different calcium concentrations, in the most prominent applications besides milk, films containing caseins are used. Casein adhesives hold the unchallenged top position regarding labeling of glass containers. For labeling of beverage containers, preserve jars, and other containers, this natural product is most widely used. Particularly if glass surfaces are to be coated, if they are subject to condensation or ice water or if labels are to be applied to extremely cold containers, casein-based adhesives are the first choice. Moreover, comparable to other biopolymer systems, such as membranes, thin film investigations open an alternative approach for structural studies. Recently, spin-coating was shown to be an efficient technique to prepare well-defined casein films of controllable thickness over a wide range of different pH values (26). At high concentrations with spin-coating, bulklike films are prepared, which structure matches well the micellar structure in solution. In contrast to the long times required for drying in the solution casting technique, spin-coating is very quick. After 30 s only, a well-defined, homogeneous, and dry film of very high quality is obtained.

Within the present investigation we focus on the effect of calcium concentration on the structure of casein micelles in thin films (prepared by spin-coating). $CaCl_2$ was added, at room temperature, to casein micelles extracted from commercial-grade skim milk in a concentration range from 0 to 100 mM. As reference for the thin film investigation, bulk solutions were probed with static and dynamic light-scattering experiments. To avoid problems related with dilution, native turbid solutions were analyzed at a concentration of 3%, using a backscattering technique, which records only light scattered from the surface of the sample. This procedure minimizes multiple scattering and yields approximate molecular parameters even of turbid solutions. The thin film investigation is based on grazing incidence small angle x-ray scattering (GISAXS) and complemented with optical microscopy and atomic force microscopy to picture the surface structure.

After a short introduction to the basic experimental methods, light scattering, atomic force microscopy, and grazing incidence small angle x-ray scattering, the influence of added calcium for a fixed film thickness is discussed. A summary concludes the article.

MATERIALS AND METHODS

Sample preparation

Casein micelles were extracted from commercial-grade skim milk by a combined uniform *trans*-membrane pressure microfiltration (mean pore diameter 0.1 μm) and ultrafiltration, concentrated by five washing steps and dried in a spraying tower (27). Casein powder was dissolved in filtered 0.1 M Mes/Tris-HCl solution, at a concentration of 100 mg/ml. The pH was adjusted to 7.3 with HCl. The solutions were equilibrated by thoroughly stirring for 5 h at 293 K. To adjust the desired calcium concentration, $CaCl_2$ was added, at room temperature, in a concentration range from 0 to 100 mM. For the static and dynamic light-scattering experiments, a reduced casein concentration of 30 mg/ml was prepared by the addition of purified water.

Casein films were prepared by spin-coating (2000 rpm, 30 s) onto precleaned glass slides (28–31). For cleaning, the glass slides were placed in dichloromethane in an ultrasonic bath for 5 min and rinsed with Millipore water shortly after (Millipore, Billerica, MA). Afterwards, the glass substrates were kept for 2 h in an oxidation bath at 75°C consisting of 1400 ml Millipore water, 120 ml H_2O_2 and 120 ml NH_3 to clean the surface from organic traces. Thereafter the samples were stored in Millipore water. Directly before spin-coating the glass slides were rinsed with Millipore water for at least five times to remove possible traces of the oxidation bath. The samples were dried using compressed nitrogen before coating the glass surface.

The samples were freshly prepared in advance of the scattering experiment. Dry films were investigated resembling the final state being present in applications.

Light scattering

Static and dynamic light-scattering experiments (photon correlation spectroscopy, i.e., PCS) were performed with an ALV-NIBS System (ALV-Laser, Langen, Germany) using the light of a He–Ne laser (model No. 1145P, JDS Uniphase, Milpitas, CA) at a wavelength of 632.8 nm and 22 mW power. The temperature was stabilized by a thermostat bath at 20°C. The back-scattered light is recorded in a 177° back-scattering geometry using a sensitive avalanche diode as detector. The resulting signal is transmitted to a multiple timescale correlator (model No. ALV-5000; ALV-Laser). The back-scattering setup with turbid casein solutions (at a concentration of 3%) yielded almost identical size distributions to those derived from more dilute (0.5%) samples (32, 33). Multiple scattering enhances the initial decay of the intensity correlation function, which leads to a bias in the size distribution toward smaller values.

Particle size distributions at various Ca concentrations were calculated by transforming the intensity-intensity correlation functions with the CONTIN 2DP routine (34), implemented in the ALV data analysis package.

Optical investigation

The sample surfaces were observed with optical microscopy using an Axiotech model No. 25H optical microscope (Zeiss, Oberkochen, Germany) with magnifications between 4 and 100×. A model No. KP-D50 CCD camera recorded the micrographs (Hitachi, Tokyo, Japan).

Atomic force microscopy

An Autoprobe CP (Veeco, Plainview, NY) atomic-force microscope (AFM) was used for the investigation of the casein film surfaces. The operated gold-coated silicon cantilevers (Veeco) with a spring constant of $\cong 2.1$ Nm^{-1} had a high aspect ratio. The tips had a typical radius of curvature of 10 nm, which is small compared to the structures measured. All measurements were performed under air and at room temperature. The AFM height and lateral calibration was performed several times with calibration standards to improve the accuracy of the height and lateral information. Due to the hardware linearization of our AFM system this calibration works over the covered range of heights and surface areas. Each scanned micrograph consists of 256 lines, scanned with 0.25 Hz up to 1.0 Hz. Several images were measured for each sample. Micrographs were recorded at different sample positions in noncontact mode. Contact avoidance to the sample minimized the tip-induced sample degradation. At each individual sample position

scans with different ranges from 1 μm $\times$ 1 μm up to 10 μm $\times$ 10 μm were performed. From the raw data, the background due to the scanner tube movement was fully subtracted to determine the values of the root-mean-square roughness over the complete scan area.

Grazing incidence small-angle x-ray scattering

To probe structures inside the casein films, grazing incidence small-angle x-ray scattering (GISAXS) was applied (35–37). The GISAXS experiments were performed at the BW4 beamline at the synchrotron HASYLAB (DESY, Hamburg, Germany) (38). The selected wavelength was $\lambda = 0.138$ nm. A setup of high quality entrance slits and a completely evacuated pathway was used. The two entrance cross-slits defined the beam divergence in and out of the plane of reflection to match the desired resolution. The samples were placed horizontally in the GISAXS sample chamber at 2.2-m distance from the two-dimensional detector (MARCCD, 2048 $\times$ 2048 pixels). The GISAXS signal was recorded at one fixed angle of incidence α_i = 0.466°. In front of the detector two separate beam-stops were installed at the position of the direct beam and the specular peak to shield the detector. A detailed description of GISAXS as an advanced scattering technique for the investigation of nanostructured polymer films is given in Müller-Buschbaum (37). The two-dimensional intensity distribution can be understood as an assembly of several vertical and horizontal slices (35).

RESULTS

Solution structures

Dynamic and static light-scattering experiments (PCS) were performed at 177° with turbid casein solutions at various calcium concentrations. Dust particles in the sample volume are a major complication of light-scattering studies. Usually, careful filtering procedures have to be applied. However, in the case of casein micelles an efficient filtering is not possible, since dust particles and micelles are of similar size. It is thus essential to work with concentrated solutions of dust-controlled casein preparations (filtered buffers). This guarantees that the scattering signal of casein dominates with respect to the signal of the buffer (33).

Fig. 1 shows the effect of calcium addition probed with PCS. In Fig. 1 *a*, the intensity autocorrelation functions of the light scattered from a casein solution with and without calcium are displayed. With CaCl$_2$ added, the characteristic decay time shifts toward larger values directly visualizing the increase in micelle size. The resulting *z*-averaged radial size distribution $P(r)$ obtained by direct (''unweighted'') inversion of the correlation function are shown in Fig. 1 *b*. The

z-averaged distribution is biased in favor of massive particles $\cong nM^2$, with M denoting the molecular weight and n the number density.

Based on a cumulant expansion (39), the average diffusion coefficient D is determined from the initial slope of the intensity correlation function versus time. Assuming homogeneous spherical particles the apparent hydrodynamic radius R_H is derived from the Stokes-Einstein relation $D = k_B T/(6\pi\eta R_H)$, where k_B denotes the Boltzmann's constant and η the viscosity. In polydisperse systems a distribution of relaxation times is required. Without added calcium the most probable radius is 130 nm in good agreement with previous investigations (26,40). The broad size distribution of the casein micelles, shown in Fig. 1 *b*, is a characteristic feature of casein micelles. If considered as a Gaussian distribution, the polydispersity is ~50%, which is very large as compared to other biological systems, but smaller than that of emulsions (32). With 10 mM Ca added, the most probable radius increases slightly to 140 nm. Upon further increase of the amount of added calcium, an increase in micelle radius up to a value of 315 nm is obtained (at 110 mM Ca added). The width of the size distribution remains broad irrespective of the Ca concentration. Since native micelles at ambient pressure are comparable in size to the wavelength of light (200 vs. 600 nm), intramolecular interference effects cannot be ignored. This effect can lead to size distributions, which depend on the scattering angle, emphasizing smaller particles at high scattering angles. As a consequence, the shown size distribution might be artificially broadened at small radii and thus overestimate the real polydispersity of the casein micelles. However, both size distributions in Fig. 1 *b* show the presence of smaller, $\cong$20-nm-sized (diameter) species. Instead of a micellar substructure, this indicates the presence of significantly smaller micelles. These mini-micelles are in coexistence with the typically reported larger casein micelles.

Thin film structures

Being a very powerful technique in the field of synthetic polymer film preparation (28–30), recently spin-coating was shown to enable the preparation of thin and homogeneous casein films (26). A pretreatment of the glass substrates used
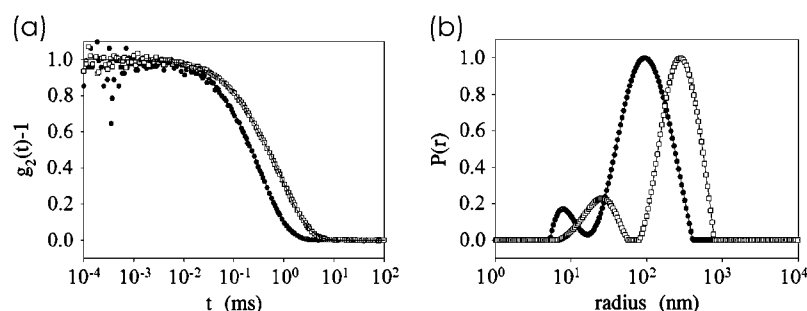

FIGURE 1   (*a*) Intensity correlation function of light scattered from casein solutions with (*open squares*) and without (*solid circles*) Ca shown together with a fit calculated from the radial size distribution. The measurement was performed in backscattering geometry (177°). (*b*) Unweighted or *z*-averaged radial size distribution $P(r)$ shown as a function of a logarithmic radius r. Data without the addition of Ca (*solid circles*) and with 100 mM Ca added (*open squares*) are compared as examples.

for the spin-coating is a key part in the preparation. The applied base bath ensured wettability of the glass surface by the water-based casein solution. At the selected high concentration of casein of 100 mg/ml, thick homogenous films result. Over a large range of pH from 5.1 to 9.4 the structural characteristics of the casein micelles in spin-coated films agree very well with the average diameter of casein micelles in solution (26).

A visualization in real space is obtained with AFM. Fig. 2 shows topographic data of casein films spin-coated out of solutions with different added amount of Ca on a scan range of $5 \times 5 \ \mu m^2$. In all images the surface shows the presence of packed casein micelles with one dominant size (and of course a size distribution). With increasing amount of Ca, the number and size of large aggregates coexisting with the micelles increases. For example, at 100 mM Ca (Fig. 2 d) very clearly two types of Ca micelles are observable. The distance between the dominant casein micelle types is 160 nm. The size of the large aggregates agrees well with a diameter of ~600 nm and thus very well with the observations from solution.

In Fig. 2, regions of mini-micelles, which are observed with PCS, are not visible due to the large scan range. To resolve structures of ~20 nm, a smaller scan range is necessary. However, with decreasing scan range, the statistical significance of the individual images decreases. To demonstrate this, Fig. 3 shows two representative AFM images with a scan range of $1 \times 1 \ \mu m^2$. In Fig. 3 a, the micelles dominating the images shown in Fig. 2 are visible. No big aggregate is included in the scan range and in the central part of the image one might be tempted to see a significantly smaller micelle type, the mini-micelles. Nevertheless, in the rest of the image, no mini-micelles can be
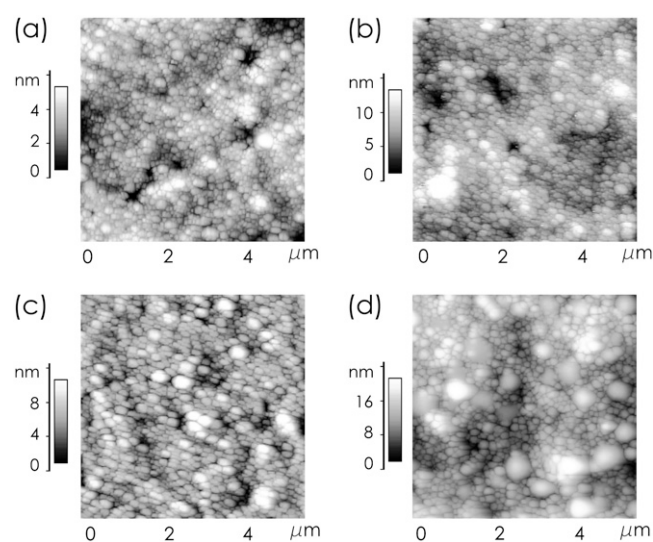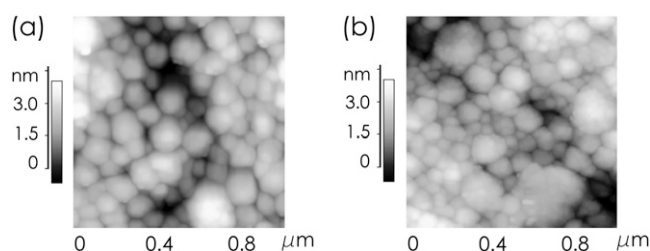

FIGURE 3 High-resolution AFM topography images showing the surface of spin-coated casein films with 60 mM Ca added at two different positions (a) without and (b) with regions of mini-micelles.

found. Fig. 3 b suggests a different view: On this spot of the sample regions covered with mini-micelles are easily observed.

Fig. 4 shows examples of line cuts from the AFM topography data. The height profile line exhibits, on a large scan range of 5 μm, the coexistence of casein micelles (denoted with II in Fig. 4 a) with large aggregates (denoted with I). At the selected example of 60 mM calcium, the distance between neighboring casein micelles is 160 nm and the aggregates have ~500 nm diameter. In the height profile line on a smaller scan range of 1 μm, in addition to the micelles (denoted with II in Fig. 4 b), the coexisting mini-micelles with a nearest-neighbor distance of 50 nm are visible. However, in line cuts, the aggregates, micelles, and mini-micelles are not always cut in the center, which causes deviations from the given values. Moreover, statistics are very limited.

Whereas AFM and optical microscopy show the casein film surface in real space, GISAXS has proven to be excellently suited to access the internal film structure. Fig. 5 shows a typical two-dimensional GISAXS pattern. Characteristic features are the specular peak, hidden behind a beamstop to protect the sensitive detector, and the Yoneda peak (41). The polydisperse casein micelles give rise to a strong diffuse scattering, whose characteristic triangular shape (visible by the green color) is not qualitatively affected by the addition of calcium. Thus Fig. 5 gives a very good impression of the typical two-dimensional intensity distribution recoded in a GISAXS experiment. Instead of modeling the full two-dimensional intensity distribution (42), the analysis is restricted to horizontal line cuts (called "out-of-plane scan"). These line cuts (out-of-plane scans, respectively) contain scattering contributions with in-plane information only. Because the flat glass surface gives no contribution with a marked intensity distribution to the diffuse scattering, the probed signal originates from the casein film structure only (26).

Fig. 6 shows out-of-plane scans for nine different calcium concentrations. The diffusely scattered intensity is shown as a function of scattering vector component q_y. The coordinate system is chosen that the film surface is in the (xy)-plane and the x-ray beam is directed along the x axis. Thus structures

FIGURE 2 AFM topography images showing the surface of spin-coated casein films with (a) 10, (b) 20, (c) 60, and (d) 100 mM Ca added.
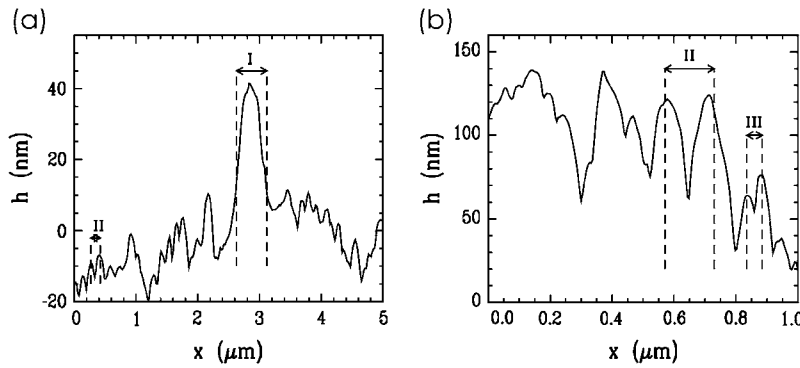
FIGURE 4 Line cuts from the AFM topography data of spin-coated casein films with 60 mM Ca added displaying (*a*) coexistence of large aggregates (marked with *I*) and casein micelles (marked with *II*) and (*b*) coexistence of casein micelles (marked with *II*) and mini-micelles (marked with *III*).

perpendicular to the x-ray beam and parallel to the film surface are probed with GISAXS. In Fig. 6, from the bottom to the top, the amount of added $CaCl_2$ increases from 0 to 100 mM. With respect to the qualitative shape, all out-of-plane scans are similar: At very small q_y-values, close to the resolution limit (shown with the *dashed line*), the intensity rises strongly due to the presence of large scale lengths describing the assembly of the casein micelles as visualized on the surface by AFM. At large q_y-values, corresponding to distances of $\cong 20$ nm, a well-pronounced peak is visible. The position of the peak shifts as a function of the Ca concentration. In addition, a shoulder-like intensity decay is located between both regions.

For a quantitative description, the GISAXS data are fitted with a simple model (43). In contrast to standard transmission experiments probing bulk volumes, in GISAXS the scattered intensity is complicated by reflection and refraction effects (44,45). In a simplified expression, the scattered intensity can be written as (45)

$$I(\alpha_f, \psi) \cong \frac{1 - \exp[-2\,\Im(q_z)d]}{32\pi^2\,\Im(q_z)}I_4, \qquad (1)$$

accounting for the four characteristic contributions arising from: scattering; scattering and reflection; reflection and scattering and reflection; and scattering and reflection, given with

$$I_4 = |T_iT_f|^2 I_t(q_\parallel, \Re(q_{1,z})) + |T_iR_f|^2 I_t(q_\parallel, \Re(q_{2,z})) \\ + |R_iT_f|^2 I_t(q_\parallel, \Re(q_{3,z})) + |R_iR_f|^2 I_t(q_\parallel, \Re(q_{4,z})). \qquad (2)$$

Here, $\Re(x)$ is the real and $\Im(x)$ is the imaginary part of x. $R_{i,f}$ and $T_{i,f}$ are the reflected and transmitted amplitudes of the incoming (*i*) and outgoing (*f*) x-ray beam. With $k_o = -2\pi/\lambda$ and the z-components of the incoming (*i*) and outgoing (*f*) x-ray beam $k_{z,i,f} = k_o\sqrt{n^2 - cos^2(\alpha_{i,f})}$ the scattering vector $\vec{q}$ is defined with components, $q_\parallel = \sqrt{q_x^2 + q_y^2}$, $q_{z,1} = k_{z,f} - k_{z,i}$, $q_{z,2} = -k_{z,f} - k_{z,i}$, $q_{z,3} = k_{z,f} + k_{z,i}$, and $q_{z,4} = -k_{z,f} + k_{z,i}$. In Eq. 2 the shape of the micelles enters via a form-factor contribution $P(\vec{q})$ and the distance between neighboring micelles via a structure factor contribution $S(\vec{q})$ with

$$I_t = P(\vec{q})S(\vec{q}). \qquad (3)$$

Due to the large polydispersity as probed by DLS, no special form factor was included (26). Two characteristic lengths are modeled as structure factors broadened with a Gaussian distribution function. The experimental resolution is taken into account by a stretched Lorentzian-type distribution, as it was experimentally probed. The solid lines in Fig. 6 show the best fits obtained within this model. The data are well described within a wide q_y-range. Deviations between data and model fit occur at small q_y-values close to the resolution limit. This might be taken as a signature of the existence of well-defined large structures. However, the determination of the two characteristic lengths, described above, is not affected by this deviation.

DISCUSSION AND CONCLUSION

Grazing incidence small-angle x-ray scattering data, combined with static and dynamic light-scattering data and accompanied with atomic force microscopy and optical microscopy, provide insights into architecture and size of casein micelles at different calcium concentrations. In
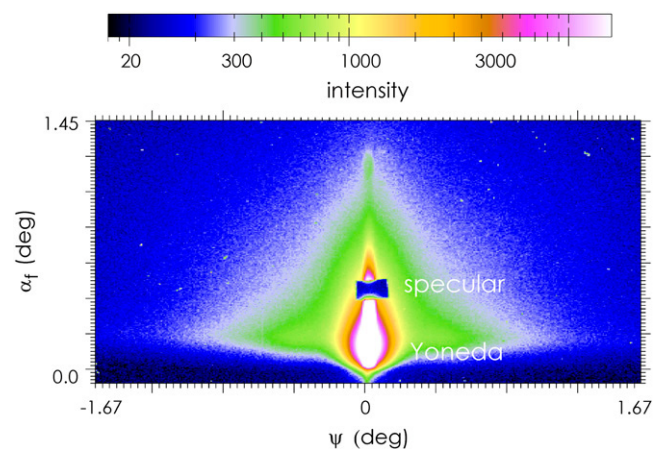

FIGURE 5 Typical GISAXS scattering signal (intensity as a function of the exit angle α_f and the out-of-plane angle Ψ) recorded with a two-dimensional detector. The shown region of interest was cut from larger detector area. At the chosen incident angle the Yoneda peak and a specular peak are well separated along the scattering plane.
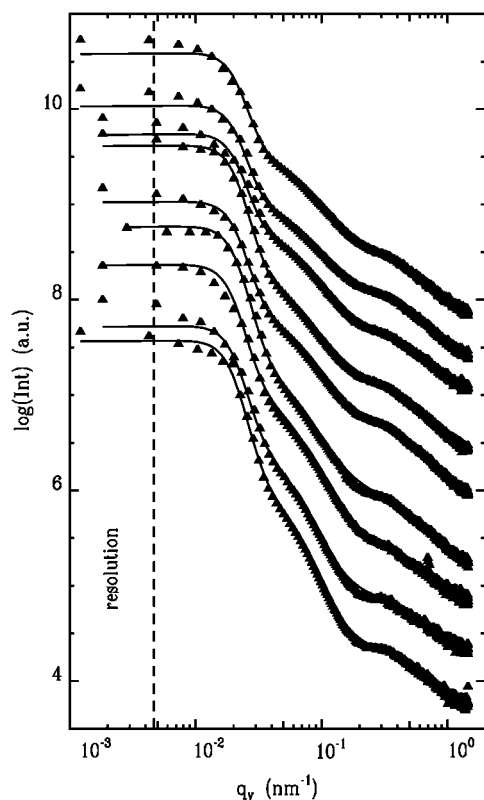
FIGURE 6 Double logarithmic plot of the horizontal line cuts from the two-dimensional GISAXS signals (*solid triangles*) measured at casein films prepared at different Ca concentrations together with model fits (*solid lines*) as explained in the text. From the bottom to the top the added amount of Ca increases from 0 to 100 mM in steps of 10 mM (except 70 and 90 mM). The curves are shifted along the *y* axis for clarity. The resolution limit toward large length scales is shown by the dashed line.
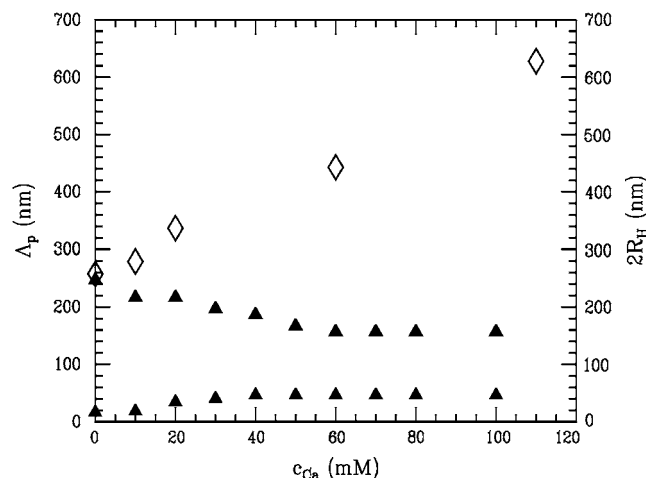

FIGURE 7 Influence of added Ca on the size of the casein micelles in solution as probed by PCS revealing the hydrodynamic diameter $2R_H$ (*open diamonds*). For comparison, the distance between neighboring micelles in dry casein films as probed with GISAXS corresponding to the most prominent in-plane length Λ_p (*solid triangles*) is shown.

particular, the comparison between bulk solution and thin film properties allows discriminating between reversible and irreversible structural changes.

Fig. 7 comprises the structural information resulting from PCS (*open symbols*) and GISAXS (*solid symbols*). Without added calcium, within the experimental error, both techniques yield a good agreement between the hydrodynamic radius, determined with PCS, and the distance between neighboring casein micelles, probed with GISAXS. Such agreement was observed in previous work as well (26) and translates into densely packed micelles (similar to hard spheres), which are unchanged by the spin-coating.

The α(s1,2)- and β-caseins mainly make up the interior, while κ-casein is located on the surface of the micelle. The κ-caseins can be regarded as block copolymers, with a block adsorbed in the micelle and a nonadsorbed block sticking into the solution. The C-terminal end of the κ-caseins supposedly extends into the solution and forms a so-called hairy layer (32). This hydrophilic layer, common to all models, prevents unlimited growth of the micelle by shielding further hydrophobic contacts. Comparable to a salted extended polyelectrolyte brush, the hairy layer of

κ-caseins is negatively charged. The resulting repulsive interaction prevents a merging of neighboring casein micelles. Because ionic strength is high, there is no long-range repulsion and casein micelles can be considered as hard sphere particles (32).

In addition, GISAXS detects a smaller structural feature of 20 nm size. At this typical length, small-angle x-ray scattering (46,47) and small-angle neutron scattering (48–50) experiments had detected a scattering feature as well (14). In literature, this feature was interpreted as a substructure of the casein micelle. In the framework of the sub-micelle model (11–13), subunits of 15–20 molecules each aggregate via hydrophobic interaction into a well-defined substructure on a scale of 20 nm. These sub-micelles act as building blocks and, linked by small calcium phosphate clusters, from the casein micelles. Alternatively, calcium phosphate ion nanoclusters were assumed to form a disordered array with a characteristic correlation length of ~20 nm (14). The calcium phosphate clusters act as seeds of micelle growth (14,15) and within a casein micelle of ~1000 of such clusters are grouped. However, instead of a well-ordered internal structure of the casein micelles, the structural feature of 20 nm might be explained with additionally present smaller species. Such mini-micelles are detected in our PCS and AFM experiments as well. Their detection in GISAXS implies, on the one hand, the existence of a large number of such mini-micelles and, on the other hand, the presence of regions, in which the mini-micelles are densely packed. Moreover, from the detection of two characteristic lengths it can be concluded, that micelles and mini-micelles exist in coexistence in solution and in the casein films.

The colloidal properties of casein micelles change with the addition of calcium. After addition of calcium, PCS detects a

strong increase in the hydrodynamic radius (see Fig. 7). In contrast, GISAXS shows a slight decrease in the micelle distance together with an increase in the smaller structural feature. The increase in hydrodynamic radius agrees with previous investigations (24,51,52). By adding a small amount of calcium, solvable caseins initially increase the micellar weight without increasing the size (51), as long as the casein micelle can incorporate calcium-insensitive caseins (α(s1,2)- and β-caseins). Upon further addition of calcium, the radius of the micelles increases up to a critical concentration. Above this critical concentration the addition of calcium causes gross aggregation and precipitation of the micelles (51). Within this work, the critical concentration of precipitation was >110 mM.

In the framework of the adhesive hard sphere model (53), the steep repulsive interaction of two micelles is preceded by a short-range van der Waals attraction (21). The addition of Ca changes this equilibrium. The negative charge of the extended polyelectrolyte brush is reduced, κ-caseins associate at the micelle surface, and the brush loses its extended conformation. As a consequence, the particle-stabilizing properties of the hairy layer are lost and attraction between neighboring micelles becomes noticeable. Micelles can associate and build aggregates with larger hydrodynamical radii. Being dependent on the charge density along the chains of the κ-caseins, the same behavior occurs by lowering the pH of casein solutions (19–21).

Related to the thin casein films prepared by spin-coating this micelle aggregation does not translate in a similar increase in the characteristic distances. Fig. 8 sketches two limiting cases: Fig. 8 *a*, without added calcium, the casein micelles are covered by a hairy layer of κ-caseins; and Fig. 8 *b*, at high added calcium concentration, this κ-casein layer has collapsed and neighboring micelles aggregate. GISAXS detects distances between adjacent micelles (26) and thus the collapse of the extended polyelectrolyte brush directly translates into a decrease in the distances of neighboring micelles. With increasing Ca concentration, PCS and GISAXS (and AFM) yield diverging values of the hydrodynamic radius R_H and of the distance Λ_p (see Fig. 7). The presence of large aggregates, which is probed with PCS and AFM, is not detected in GISAXS, because it adds no further dominant length visible in GISAXS. With respect to the resolution limit of GISAXS toward large objects (as

indicated by the *dashed line* in Fig. 6), the numbers detected with PCS and AFM would have been easily resolved (54,55). However, as mentioned before, polydispersity prevents the observation of the object shape in GISAXS (56). Consequently, in GISAXS, individual casein micelles are probed and the observed distances (see Fig. 8) can be understood as distances between neighboring micelles. At 60 mM Ca an equilibrium value of 160 nm is reached, which is not further decreasing with further addition of calcium.

The mini-micelles give rise to the second characteristic length observed in GISAXS and AFM. As a function of added amount of Ca, the second, smaller structural feature observed in GISAXS behaves oppositely to the casein micelles. As displayed in Fig. 7, an increase from 20 to 50 nm is observed, when Ca is added. Returning to dynamic light scattering in Fig. 1 *b*, it was found that the increase of the smaller component was quantitatively identical. Following the suggested model of mini-micelles, this translates into an increase in the distance of neighboring mini-micelles and consequently in a swelling of the mini-micelles. Thus with addition of Ca the mini-micelles start to incorporate casein molecules (57). At 40 mM Ca, this process stops and the mini-micelles stay unchanged in size.

In the framework of the sub-micelle model (11–13), this increase, as observed with GISAXS, implies an increase in the size of the sub-micelles; and in the framework of the calcium phosphate ion nanoclusters model (14–17), it would originate from an increase in the distance between these nanoclusters. That addition of calcium results in the increase between calcium nanoclusters might be unlikely. The increase in size of building blocks forming the casein micelle contrasts with the observed decrease in the large structural length in GISAXS. Thus our thin film data challenge both models—the nanocluster model and the sub-micelle model.

SUMMARY

With GISAXS and AFM, thin casein films prepared with spin-coating are investigated. The probed structures are compared with the structures present in the solutions used for spin-coating. Ca was added to the solutions within the regime, which does not include precipitation. The addition of Ca changes the equilibrium between the steep repulsive interaction of two micelles and a short-range van der Waals
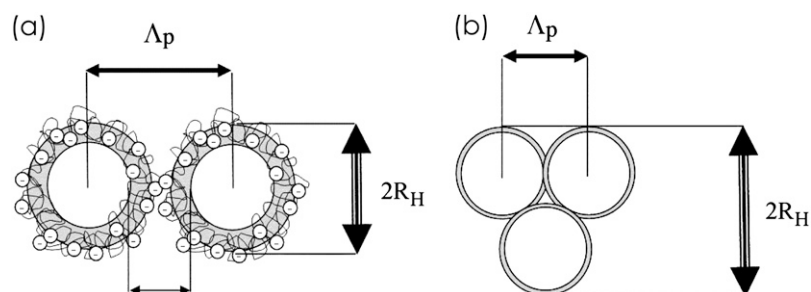

FIGURE 8 Model sketch explaining the structural features observed with PCS, GISAXS, and AFM. (*a*) Without added Ca; (*b*) with 100 mM Ca added.

attraction. With increasing amount of Ca added, the particle-stabilizing properties of the hairy layer of κ-casein become weaker and attraction between neighboring micelles becomes noticeable. Micelles can associate and build aggregates with larger hydrodynamical radii as observed in solution. In the thin films, these aggregates are not dominant in number, but individual micelles are the dominant species. These micelles are close packed, but not merged into new very big micelles. It appears clear that the observed decrease in casein micelle correlation length is caused by calcium-mediated transition from an expanded to a collapsed κ-casein salted brush. As a consequence, casein micelle size and distances between neighbored micelles decrease (19–21).

In addition to these structures created by the commonly observed casein micelles, a further type with significantly smaller diameter is probed. These mini-micelles are observed in solution as well as in the thin films. AFM allows us to visualize them on the casein film surface directly and GISAXS proves the statistical relevance of this type of micelle. Both micelle types—the mini-micelles (20-nm diameter without added Ca) and the commonly observed micelles (260-nm diameter without added Ca)—coexist. In solution this might be a dynamical equilibrium, with an exchange of caseins between individual micelles. In contrast, in thin films, a snapshot of this equilibrium is frozen in place, and aggregates, micelles, and mini-micelles are all detected. Thus, in general, the investigation of thin (casein) films allows us to probe a well-defined state of a dynamical equilibrium. In future experiments, the influence of outer parameters such as temperature and ionic strength are worth investigation.

GISAXS has proven to be a very powerful experimental technique to investigate thin biopolymer films. Due to its high sensitivity and statistical significance of the extracted structural parameters, GISAXS is extremely well suited to probe complex structures. However, due to the necessity of having access to GISAXS, this approach is limited to large scale facility research.

REFERENCES

1. Farrell, H. M., Jr. 1988. Physical Equilibria: Proteins. *In* Fundamentals of Dairy Chemistry, 3rd Ed. N. Wong, editor. Van Nostrand-Reinhold, New York.

2. Holt, C. 1992. Structure and stability of bovine casein micelles. *Adv. Protein Chem.* 43:63–113.

3. Holt, C., and L. Sawyer. 1988. Primary and predicted secondary structures of the caseins in relation to their biological functions. *Protein Eng.* 2:251–259.

4. van Kemenade, M. J. J. M., and P. L. de Bruyn. 1989. The influence of casein on the kinetics of hydroxyapatite precipitation. *J. Colloid Surface Interf. Sci.* 129:1–14.

5. Walstra, P., and R. Jenness. 1984. Dairy Chemistry and Physics. Wiley, New York.

6. McMahon, D. J., and W. R. McManus. 1998. Rethinking casein micelle structure using electron microscopy. *J. Dairy Sci.* 81:2985–2993.

7. DeKruif, C. G., and C. Holt. 2003. Advanced Dairy Chemistry, Vol. 1: Proteins, 3rd Ed. P. F. Fox and P. L. H. McSweeney, editors. Kluwer Academic/Plenum Publishers, New York.

8. Dalgleish, D. G., P. A. Spagnuolo, and H. Douglas Goff. 2004. A possible structure of the casein micelle based on high-resolution field emission scanning electron microscopy. *Int. Dairy J.* 14:1025–1031.

9. Horne, D. S. 2006. Casein micelle structure: models and muddles. *Curr. Opin. Coll. Interf. Sci.* 11:148–153.

10. Fox, P. F. 2003. Advanced Dairy Chemistry, Vol. 1: Proteins, 3rd Ed. P. F. Fox and P. L. H. McSweeney, editors. Kluwer Academic/Plenum Publishers, New York.

11. Schmidt, D. G. 1982. Developments in Dairy Chemistry. Elsevier Applied Science, London.

12. Schmidt, D. G., P. Walstra, and W. Buchheim. 1973. Size distribution of casein micelles in cow's milk. *Neth. Milk Dairy J.* 27:128–142.

13. Walstra, P. 1999. Casein sub-micelles: do they exist? *Int. Dairy J.* 9: 189–192.

14. Holt, C., C. G. de Kruif, R. Tuinier, and P. A. Timmins. 2003. Substructure of bovine casein micelles by small-angle x-ray and neutron scattering. *Colloids Surf. A.* 213:275–284.

15. Holt, C. 2004. An equilibrium thermodynamic model of the sequestration of calcium phosphate by casein micelles and its application to the calculation of the partition of salts in milk. *Eur. Biophys. J.* 33:421–434.

16. Horne, D. S. 1998. Casein interactions: casting light on the black boxes, the structure in dairy products. *Int. Dairy J.* 8:171–177.

17. Horne, D. S. 2003. Casein micelles as hard spheres: limitations of the model in acidified gel formation. *Colloids Surf. A.* 213:255–263.

18. Holt, C., and D. S. Horne. 1996. The hairy casein micelle: evolution of the concept and its implications for dairy technology. *Neth. Milk Dairy J.* 50:85–111.

19. de Kruif, C. G. 1999. Casein micelle interactions. *Intl. Dairy J.* 9:183–188.

20. de Kruif, C. G. 1998. Supra-aggregates of casein micelles as a prelude to coagulation. *J. Dairy Sci.* 81:3019–3028.

21. Tuinier, R., and C. G. de Kruif. 2002. Stability of casein micelles in milk. *J. Chem. Phys.* 117:1290–1295.

22. Griffin, M. C. A., R. L. J. Lyster, and J. C. Price. 1988. The disaggregation of calcium-depleted casein micelles. *Eur. J. Biochem.* 174: 339–343.

23. Holt, C. 1997. –3– Lactose, water, salts and vitamins. *In* Developments in Dairy Chemistry. P. F. Fox, editor. Chapman and Hall, London.

24. Philippe, M., F. Gaucheron, Y. Le Graet, F. Michel, and A. Garem. 2003. Physiochemical characterization of calcium-supplemented skim milk. *Lait.* 83:45–59.

25. Pirkul, T., A. Temiz, and Y. K. Erdem. 1997. Fortification of yoghurt with calcium salts and its effect on starter microorganisms and yoghurt quality. *Int. Dairy J.* 7:547–552.

26. Müller-Buschbaum, P., R. Gebhardt, E. Maurer, E. Bauer, R. Gehrke, and W. Doster. 2006. Thin casein films as prepared by spin-coating: influence of film thickness and of pH. *Biomacromolecules.* 7:1773–1780.

27. Tolkach, A., and U. Kulozik. 2005. Fractionation of whey proteins and casein-macropeptide by means of enzymatic cross-linking and membrane separation techniques. *J. Food Eng.* 67:13–20.

28. Lawrence, C. J. 1988. The mechanics of spin-coating of polymer-films. *Phys. Fluids.* 31:2786–2795.

29. Spangler, L. L., M. Torkelson, and J. S. Royal. 1990. Influence of solvent and molecular weight on thickness and surface topography of spin-coated polymer-films. *Polym. Eng. Sci.* 30:644–653.

30. Schubert, D. W. 1997. Spin coating as a method for polymer molecular weight determination. *Polym. Bull.* 38:177–184.

31. Müller-Buschbaum, P. 2003. Influence of surface cleaning on dewetting of thin polystyrene films. *Eur. Phys. J. E.* 12:443–448.

32. Gebhardt, R., W. Doster, and U. Kulozik. 2005. Pressure-induced dissociation of casein micelles: size distribution and effect of temperature. *Braz. J. Med. Biol. Res.* 38:1209–1214.

33. Gebhardt, R., W. Doster, J. Friedrich, and U. Kulozik. 2006. Size distribution of pressure-decomposed casein micelles studied by dynamic light scattering and AFM. *Eur. Biophys. J.* 35:503–509.

34. Provencher, S. W. 1982. A constrained regularization method for inverting data represented by linear algebraic or integral equations. *Comput. Phys. Comm.* 27:213–229.

35. Salditt, T., T. H. Metzger, J. Peisl, B. Reinker, M. Moske, and K. Samwer. 1995. Determination of the height-height correlation-function of rough surfaces from diffuse-x-ray scattering. *Europhys. Lett.* 32: 331–336.

36. Naudon, A., D. Babonneau, D. Thiaudiere, and S. Lequien. 2000. Grazing-incidence small-angle x-ray scattering applied to the characterization of aggregates in surface regions. *Physica B (Amsterdam).* 283:69–74.

37. Müller-Buschbaum, P. 2003. Grazing incidence small-angle x-ray scattering—an advanced scattering technique for the investigation of nanostructured polymer films. *Ann. Bioanal. Chem.* 376:3–10.

38. Roth, S. V., R. Döhrmann, M. Dommach, M. Kuhlmann, I. Kröger, R. Gehrke, H. Walter, C. Schroer, B. Lengeler, and P. Müller-Buschbaum. 2006. The small-angle options of the upgraded USAXS beamline BW4 at HASYLAB. *Rev. Sci. Instr.* 77:085106.

39. Koppel, D. 1972. Analysis of macromolecular polydispersity in intensity correlation spectroscopy: the method of cumulants. *J. Chem. Phys.* 57:4814–4820.

40. Anema, S. G., S. K. Lee, K. Schrader, and W. Buchheim. 1997. Effect of pH on the turbidity of pressure-treated calcium caseinate suspensions and skim milk. *Milchwissenschaft.* 52:141–146.

41. Yoneda, Y. 1963. Anomalous surface reflection of x-rays. *Phys. Rev.* 131:2010.

42. Müller-Buschbaum, P., N. Hermsdorf, S. V. Roth, J. Wiedersich, S. Cunis, and R. Gehrke. 2004. Comparative analysis of nanostructured diblock copolymer films. *Spectrochim. Acta B Atomic Spectrosc.* 59:1789–1797.

43. Panagiotou, P., E. Bauer, S. Loi, T. Titz, E. Maurer, and P. Müller-Buschbaum. 2004. Polymeric structures at interfaces: an x-ray scattering study. *Z. Kristallogr.* 219:210–217.

44. Holý, V., and T. Baumbach. 1994. Nonspecular x-ray reflection from rough multilayers. *Phys. Rev. B.* 49:10668–10676.

45. Lee, B., J. Yoon, W. Oh, Y.-T. Hwang, K. Heo, K. S. Jin, J. Kim, K.-W. Kim, and M. Ree. 2005. In-situ grazing incidence small-angle x-ray scattering studies on nanopore evolution in low-K organosilicate dielectric thin films. *Macromolecules.* 38:3395–3405.

46. Pessen, H., T. F. Kumosinski, and H. M. Farrell. 1989. Small-angle x-ray-scattering investigation of the micellar and submicellar forms of bovine casein. *J. Dairy Res.* 56:443–451.

47. Pignon, F., G. Belina, T. Narayanan, X. Paubel, A. Magnin, and G. Gesan-Guiziou. 2004. Structure and rheological behavior of casein micelle suspensions during ultrafiltration process. *J. Chem. Phys.* 121: 8138–8146.

48. Stothart, P. H., and D. J. Cebula. 1982. Small-angle neutron-scattering study of bovine casein micelles and sub-micelles. *J. Mol. Biol.* 160:391–395.

49. Stothart, P. H. 1989. Subunit structure of casein micelles from small-angle neutron-scattering. *J. Mol. Biol.* 208:635–638.

50. Hansen, S., R. Bauer, S. B. Lomholt, K. Bruun Qvist, S. V. Pedersen, and K. Mortensen. 1996. Structure of casein micelles studied by small-angle neutron scattering. *Eur. Biophys. J.* 24:143–147.

51. Lin, S. H. C., S. L. Leong, R. K. Dewan, V. A. Bloomfield, and C. V. Morr. 1972. Effect of calcium-ion on structure of native bovine casein micelles. *Biochemistry.* 11:1818–1821.

52. Pastorino, A. J., N. P. Ricks, C. L. Hansen, and D. L. McMahon. 2003. Effect of calcium and water injection on structure-function relationships of cheese. *J. Dairy Sci.* 86:105–113.

53. Baxter, R. J. 1968. Percus-Yevick equation for hard spheres with surface adhesion. *J. Chem. Phys.* 49:2770–2774.

54. Müller-Buschbaum, P., M. Casagrande, J. Gutmann, T. Kuhlmann, M. Stamm, S. Cunis, G. von Krosigk, U. Lode, and R. Gehrke. 1998. Determination of micrometer length scales with an x-ray reflection ultra small-angle scattering set-up. *Europhys. Lett.* 42:517–522.

55. Müller-Buschbaum, P., E. Bauer, E. Maurer, K. Schlögl, S. V. Roth, and R. Gehrke. 2006. A new route to large-area ordered polymeric nano-channel arrays. *Appl. Phys. Lett.* 88:083114.

56. Walter, H., P. Müller-Buschbaum, J. S. Gutmann, C. Lorenz-Haas, C. Harrats, R. Jerome, and M. Stamm. 1999. Lateral structures of thin films of ampholytic diblock copolymers adsorbed from dilute aqueous solution at the solid/liquid interface. *Langmuir.* 15:6984–6990.

57. Chu, B., Z. Zhou, G. Wu, and H. M. Jr. Farrell. 1995. Laser-light scattering of model casein solutions—effect of high-temperature. *J. Colloid Interface Sci.* 170:102–112.